

On topological frustration and graphene magnonics

Vasil Saroka*

V. A. Saroka

¹Department of Physics, University of Rome Tor Vergata and INFN, Via della Ricerca Scientifica 1, 00133 Roma, Italy

²Institute for Nuclear Problems, Belarusian State University, Bobruiskaya 11, 220006 Minsk, Belarus
Email Address: vasil.saroka@roma2.infn.it

Keywords: *strong correlations, quantum magnetism, graph theory, matchings, topology*

The graph-theoretic topological frustration is a peculiar situation on a finite piece of the honeycomb lattice that prevents a full pairwise coupling of the lattice sites via nearest neighbor links, even when the total number of sites is an even number. This type of frustration is inherent for organic molecules that are classified as concealed non-Kekulean hydrocarbons, representing peculiar diradicals. Here we show that this topological frustration persists in 2D systems based on honeycomb lattice. Such systems exhibit fully flat electronic energy bands located at the Fermi level. Therefore, 2D ultimately flat bands can be systematically and predictably constructed for graphene monolayer nanomeshes. These systems are prone to antiferromagnetic ordering and hybrid spin-wave excitations mixing weak ferromagnetic and strong antiferromagnetic features, which could pave the way towards low-power, compact, and ultrafast organic spintronics with near room-temperature operation.

1 Introduction

Flat bands are key for the emergence of strongly correlated physics, wherein quasiparticles interactions are stronger than typical kinetic energy given by the energy band width [1, 2, 3]. The high density of states associated with narrow band width can result in Hubbard-Mott-Stoner magnetism [4, 5, 6, 7, 8], unconventional and high-temperature superconductivity [9, 10, 11, 12, 13, 14, 15, 16, 17, 18, 19, 20], and anomalous fractional quantum Hall effect [21, 22, 23, 24, 25, 26]. Although some iconic flat band lattices, such as dice [27], Lieb [28], and Kagome [29, 30] lattices, are known for long time, the general rules for flat band construction are somewhat obscure and so far deal with very exotic examples and/or incomplete flatness [31, 32, 33, 34, 35, 36, 37, 38, 39, 40, 41, 42]. Significant numerical efforts have been undertaken to reveal potential candidates with band flatness [43]. Experimentally, the major success has been achieved with twisted layers of the honeycomb lattice [44, 45, 46, 47, 48] and Kagome lattice materials [49, 50, 51, 52, 53, 54, 55], including their supramolecular analogs [56, 57]. The recent work also reports progress towards solid state realization of the Lieb lattice [58]. A somewhat broader success in flat band design and control has been achieved with artificial systems, for example, in photonic metamaterials and optically trapped cold atoms. The latter includes dice lattice realization [59], Lieb lattice manipulation [60, 61], light-matter interaction enhancement in free-electron lasers [62], and fascinating orbital rotation in Kagome lattice [63].

Although 3D [64, 65, 66] and 1D [67, 68, 69, 70, 71] flat bands can be designed, nowadays the main interest is around 2D bands due to the abundance of existing [72, 73] and newly predicted [74] 2D materials, which in a broader context are related to the practical importance of surface science and planar lithographic technology. It is important to note that there are few fundamental theorems that prohibit long-range orders in 1D and 2D systems: Lieb-Mattis theorem for ferromagnets [75], Anderson theorem for antiferromagnets [76] and Hohenberg-Mermin-Wagner theorem covering superconductors and anti-ferromagnets [77, 78]. This seems to undermine any flat band considerations beyond 3D systems. Yet, recent theoretical revisions imply that finite range orders may be macroscopically large enough in 2D [79]; alternatively, the restrictive conditions — short range interactions and continuous symmetries [77, 78] — can be bypassed by material engineering, which is in agreement with the existence of twisted bilayers [44, 46, 80] and atomically thin ferromagnets: CrI_3 [81] and $\text{Cr}_2\text{Ge}_2\text{Te}_6$ [82]. These peculiarities make the 2D flat bands extremely compelling to study.

In general, 2D flat bands can be located at any energy of the electronic spectrum. They can also have intersections with other dispersive bands. Unless the latter is a special demand, the intersections must

arXiv:2604.01227v1 [cond-mat.mes-hall] 18 Mar 2026

be avoided, so that flat bands are well isolated from the remaining spectrum, thereby enabling unambiguous detection and interpretation of the associated phenomena. In Kagome lattice, depending on the parameters of the model, the flat band is either the lowest or the highest in energy, while in the dice and Lieb lattices such a band is pinned to the Fermi level. For bosonic systems, which do not follow Pauli's exclusion principle, the flat band shall be the lowest in energy [83]. The whole-spectrum flatness may be needed to ensure a uniform response across a wide energy range of excitations [63]. However, for fermionic systems, the most attractive flat bands are those positioned at the borderline between occupied and empty states, which is referred to as the Fermi energy and commonly is set as a reference zero energy. The zero-energy states play crucial role in topological band theory via a bulk-boundary correspondence principle that predicts zero-energy states at the interfaces between the topological and trivial systems [84], therefore, it seems that topological approaches could be employed for construction of the flat bands at zero energy to achieve their stability with respect to the gentle variation of model parameters.

In the area of organic chemistry, the zero-energy states of non-Kekulean hydrocarbons [85, 86, 87, 88] are described by the graph-theoretic situation called topological frustration [89]. It is important to note that this frustration is physically different from the one studied in frustrated magnets and spin glasses [90], for example in an antiferromagnet with a triangular or Kagome lattice. In contrast to negatively coupled spins occupying *odd* number of lattice sites in the frustrated antiferromagnet, topological frustration in hydrocarbons deals with electron pairing in covalent bonds, which is certainly similar to resonating valence bond states in quantum spin liquids inspired by Pauling's theory of chemical bonds [91, 92] but will not be considered here in any substantiation, except for a few formal comments. Although electron pairing between odd number of sites is obviously impossible (*class I topological frustration* [89] or *obvious non-Kekuleans*), there exist also a more peculiar situation when electron pairing is not possible for *even* number of sites either (*class II topological frustration* [89] or *concealed non-Kekuleans*). Hereafter, by *topological frustration*, we mean class II topological frustration. At a deep mathematical level, all such frustrations are connected to the matching theory of graphs [93]. Recently, using graph theory, it has been shown that class II topological frustration is not limited to molecules, and, for example, quasi-one-dimensional polymers can exhibit it, too [94]. In fact, nothing prevents the existence of the topological frustration in two-dimensional systems either. Once there, this frustration shall forbid full electron pairing, leaving at least two lattice sites uncoupled:

$$\begin{pmatrix} 0 & f_{\mathbf{k}} \\ f_{\mathbf{k}}^* & 0 \end{pmatrix} \rightarrow \epsilon = \pm |f_{\mathbf{k}}| \quad \Rightarrow \quad \epsilon_{f_{\mathbf{k}} \rightarrow 0} = 0 \quad (1)$$

where we have written down the tight-binding model in the subspace of two coupled/uncoupled sites. If some fully coupled configuration existed, there would be possible to lift zero-energy states degeneracy and lowering the total energy of the system. However, since no coupled configurations are allowed by topological frustration, this in turn leads to fully flat k -independent electronic bands that reside at zero-energy. Note that in general accidental zeros are possible for a set of \mathbf{k}_0 such that $f_{\mathbf{k}_0} = 0$ in Eq. (1), even without topological frustration, which, in contrast, washes away the dependence on \mathbf{k} all together, i.e. $f \equiv 0$. The approach based on topological frustration shall have the advantages that the 2D flat band can be engineered in a monolayer, compared to twisted [31, 44, 47] or rhombohedral [12, 13, 34, 20] few-layer graphenes. Concurrently, topological frustration must ensure full flatness of the band, in contrast to the partial flatness predicted and later reported in a periodically strained monolayer graphene [34, 95, 96, 39].

In this paper, we show how 2D flat bands can be constructed in a systematic way on a familiar honeycomb lattice with the aid of graph-theoretic topological frustration considered on a torus instead of a plane, as is usual for hydrocarbons [86, 87], or a cylinder, as recently proposed for polymers [94]. The magnetic properties including magnon excitations are considered for such systems using the Hubbard mean-field model and linear spin-wave theory.

2 Results and discussion

2.1 Graph theory preliminaries and settings

The abstract graph theory deals with objects and the connections between them. The objects are called vertices and are depicted as points. These points can represent atomic sites in a lattice or a molecule. The connections between vertices are called edges, which are normally represented by lines, physically standing for chemical bonds. Then a graph $G(V, E)$ is a collection of vertices, V , and edges, E ; or $V(G)$ and $E(G)$, respectively, when one wants to highlight attribution to a specific graph G . By *matching* M , we denote a subset of non-adjacent edges of G . This set is referred to as *maximal matching* when it has a maximum *cardinality* $|M|$ for the given G , where $|\dots|$ denotes the cardinality – the number of elements in a set. When such a set covers all $V(G)$, then it is a *perfect matching*. The perfect matching is obviously not possible when $|V(G)|$ is odd. If $|V(G)|$ is even, $|M| = |V(G)|/2$ for the perfect matching M , while $|M| < |V(G)|/2$ for a maximum matching M . The difference $\eta = |V(G)| - 2|M|$ is called *graph deficit*. When a graph G consists of two disjoint sets of vertices A and B , it is called a *bipartite graph*. For bipartite graphs, various search algorithms are usually simpler and faster. For example, the matching set M can be found for a bipartite graph in polynomial time $O(n^{5/2})$ with Hopcroft-Karp-Karzanov algorithm [97, 98]. Bipartite graphs of a hexagonal structure correspond to benzenoid molecules and nanographenes.

Although abstract graph theory can be mapped onto real geometrical structures, in general, it does not care about geometry. For example, it does not care about edge crossings at all. Therefore, the same graph can be presented by an infinite variety of pictorial representations. Such details, however, become more important in the topological graph theory that considers graphs as embedding into some spaces, for instance, into some orientable surfaces. For the latter, graphs gain such characteristics as a crossing number, which is the minimum number of edge crossing for a planar representation of the graph, or genus, which is the genus of the orientable surface. The proper embedment in surface S implies a configuration of $V \subset S$ and $E \subset S$ that avoids crossing between E 's.

As one moves from the plane to other orientable surfaces, it becomes difficult to track the validity of even obvious statements let alone a more complex one such as existence of topological frustration. In principle, to verify topological frustration on a torus, we could come up with a formal theorem of existence like in Ref. [94]. However, here we simply present a counter example. Imagine a hexagonal bipartite (honeycomb) lattice with an even number of lattice sites on a torus, where the numbers of A and B sublattice sites are equal, i.e. $N_A = N_B$. It happens that graph-theoretic topological frustration can exist in these settings. Figure 1 (a, b), provides an apt example based on Mothra graph extended into a non-planar torus embedded graph ('Thor' graph) by locking topological frustration. The absence of perfect matching in such a graph can also be directly verified by the Hopcroft-Karp-Karzanov algorithm, which, once applied, returns the graph deficit $\eta = 2$ as seen in Figure 1(c).

An immediate consequence of this simple result is that topological frustration shall persist in doubly periodic systems having two characteristic periods. Examples are easily found among carbon nanostructures.

While carbon nanotori have structure that is different from our abstract graph, namely they require pentagons and heptagons to be introduced into the hexagonal carbon cage to realize bending at a few nanometer scale [99, 100], double periodicity is a key feature of carbon nanotubes. This means, for example, that topological frustration can be generated in straight armchair carbon nanotubes by selective carving of their surface as depicted in Figure 1(d). It is worth noting that the structure in Figure 1(d) corresponds to the armchair single-walled carbon nanotube (6,6), which has been chiral-selectively synthesized by atomically precise bottom-up growth [101]. This can be considered as a first step towards carved tubes. The second step could probably be accomplished by some kind of molecular surgery similar to that applied to produce endohedral fullerenes [102]. On the other hand, long enough nanotubes can be bent into tori as shown in Figure 1(e) without introducing defects in the hexagonal lattice structure [103], because curvature strain is inversely proportional to the radius of bending [104]. Finally, graphene nanomeshes (GNM) and patterned graphene are also viable candidates. One of them is explicitly pre-

sented in Figure 1(f).

The adjacency matrix of a graph with N vertices is a $N \times N$ matrix of 0's and 1's, wherein rows and columns have one-to-one correspondence to vertices through their enumeration and 1's occupy elements standing at the intersection of the rows and columns corresponding to vertices linked by an edge. The eigenvalues of an adjacency matrix form a spectrum of the graph it belongs to. This spectrum is equivalent to the eigenenergies of a quantum mechanical Hamiltonian. The Thor graph has two zero eigenvalues in its spectrum. This is aligned with the graph deficit $\eta = 2$. Thus, unlike its cousin Mothra graph, the Thor graph follows the nullity theorem for hexagonal graphs [105]. In other words, the Thor graph does not feature in the spectrum supernumerary zeros that are generically allowed for bipartite graphs and have been reported for hexagonal graphs with a periodic boundary condition being imposed along a single direction [94, 106].

Figure 1(e) presents a torus that is much larger than the single unit for which topological frustration is demonstrated. Our assertion that this structure preserves frustration of the original graph requires justification. For this, we need to explain how the original graph was constructed with the help of the so-called *extension rules* [94], which can be further applied to extend the graph to infinitely many structures of various sizes, including that depicted in Figure 1(e).

Figure 2 shows Tutte-Berge decomposition of the Mothra graph, combined with Gallai-Edmonds decomposition, to which we applied the extension rules. In brief, the graph theory theorems of Tutte [107] and Berge [108, 109], state that

- (i) a perfect matching in the graph is impossible if there is a subset $S \subset V(G)$, for which the number of odd subgraph components in $G - S$ graph is such that $c_{\text{odd}}(G - S) > |S|$,
- (ii) given (i), the graph deficit $\eta(G)$ attains maximum on S and S is called an *obstruction* or barrier.

The Gallai-Edmonds structural theorem [110] provides a way to build a canonical obstruction A , which may be different from S , shedding light on odd and even subgraph components of the graph $G - A$ and consequently on $G - S$ in general. For example, even components of $G - S$ are those vertices $C(G)$ that remain covered by all possible maximum matchings M 's of G . The structural decomposition of the starting graph is presented in Figure 2(a). The extension rules are simple observation that *adding an even number of vertices to any subgraph component of $G - S$ does not violate Tutte's criterion*, as demonstrated in Figure 2(b). The large torus in Figure 1(e) is one of the possible extensions of $C(G)$ with an even number of new vertices.

In a less technical way, we have seen that graph theory provides a comprehensive formalism and a reliable set of theorems for tracking and handling topological frustration in bipartite graphs, including those composed of the integer number of hexagons of a honeycomb lattice. Specifically, topological frustration boils down to a collection of sites that form an obstruction for the lattice site pairwise coupling. This collection of sites stays invariant if the piece of lattice in question that forms the nanostructure is extended further into the lattice, keeping the even-odd parity balance with respect to structural components surrounding the obstruction. This freedom allows one to extend nearly any finite hydrocarbon into a two dimensional graphene nanomesh predicting a fully flat band.

2.2 Flat bands and emergent quantum magnetism

In the previous section, we have seen that the GNM based on the Thor graph, shown in Figure 1(f), is characterized by topological frustration. From the quantum chemistry point of view, this means that the structure shall exhibit properties of a concealed non-Kekule diradical; it is also quite natural to ponder of the lattice of the coupled spins, but we refrain from such considerations here and rather focus on emergent magnetism that will be further reduced to the spin lattice. The presence of two zero eigenvalues in the adjacency matrix of the Thor graph also supports this idea. However, this might not be obvious to a skeptical reader. Therefore, we proceed to a direct verification using the nearest-neighbor tight-binding model (TB), also known as the Hückel model in chemistry, and a further inspection of magnetism

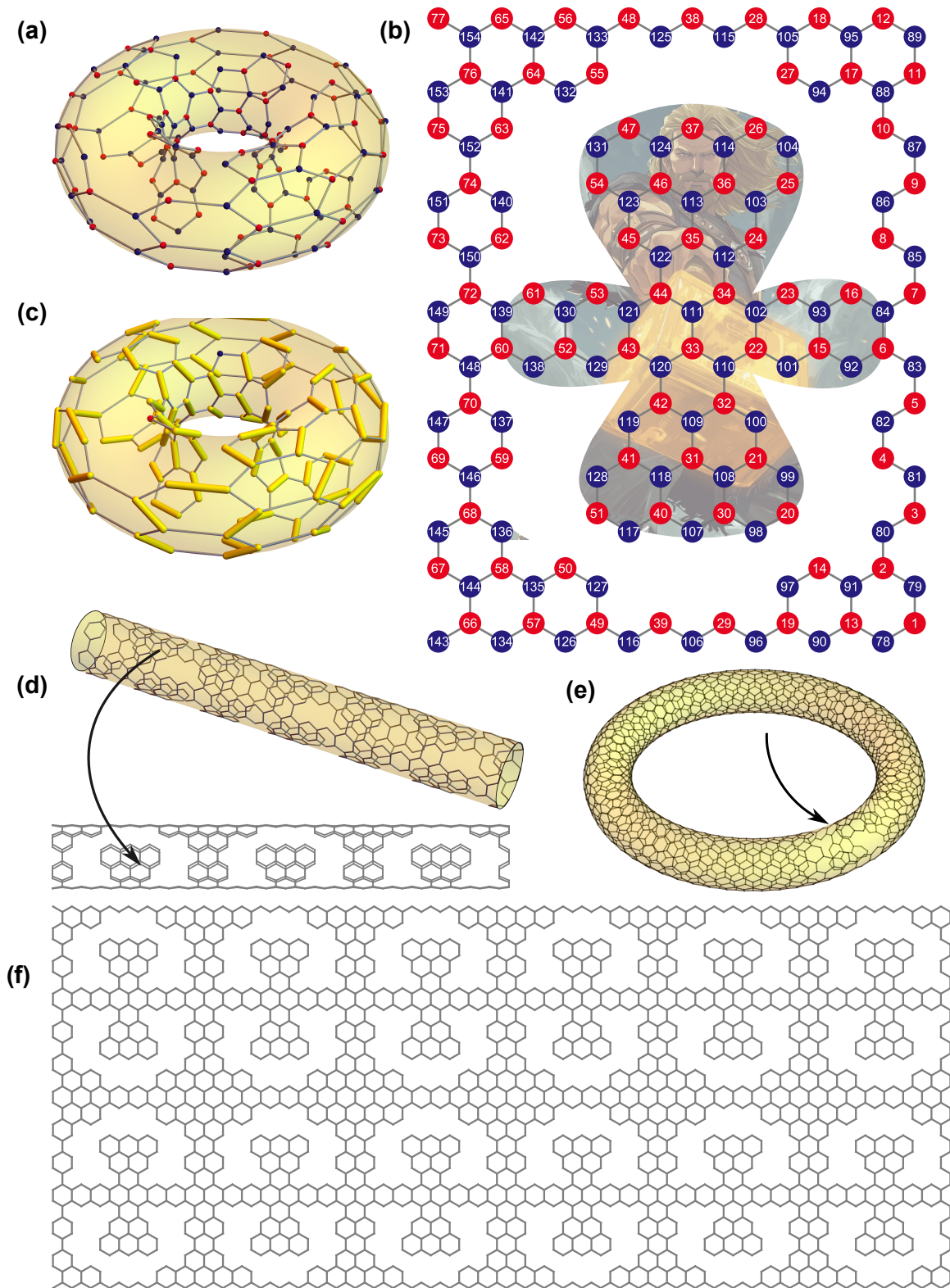


Figure 1: Topological frustration on torus. (a) A torus embedding of bipartite hexagonal graph based on Mothra [94], featuring equal number of vertices in subsets A (red) and B (blue): $N_A = N_B = 77$. (b) Mothra-based graph from panel (a) unrolled into a plane. Edges connecting bottom to top and left to the right are not shown for clarity of the picture. Vertices in A (red) and B (blue) subsets are numbered, sequentially. The AI-generated background artwork explains a formal ‘Thor’ name chosen for this graph. (c) The maximal matching (yellow) returned by Hopcorft-Karp-Karzanof algorithm. The two non-covered vertices represent graph deficit $\eta = 2$. (d) A segment of an amchair carbon nanotube (6, 6), decorated with nanocarving equivalent to the one in panel (b). A 2D side projection is shown below. Black arrow: view direction. (e) A torus based on long (6, 6) nanotube with an embedding of a single unit (black arrow) from panel (b). (f) A piece of 2D topologically frustrated graphene nanomesh, which unit cell is based on Thor-graph in panel (b).

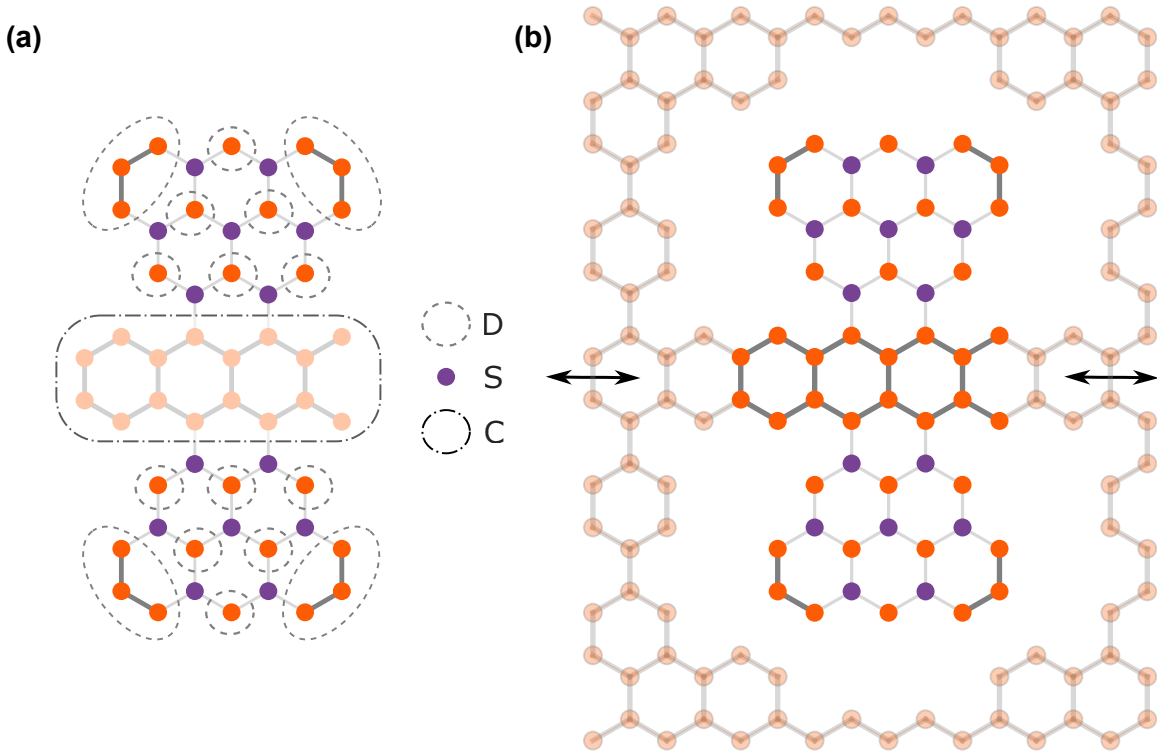


Figure 2: Obstruction and extension rules. (a) The Tutte-Berge decomposition of Mothra graph, see Ref. [94], showing obstruction set S , together with even subgraph C and odd subgraphs D . Edges incident on S are depicted with reduced opacity. (b) The Thor graph obtained by extension from the Mothra graph in panel (a) by adding an even number of vertices and edges between them, which are both highlighted as semitransparent. Black arrows: further possible extension directions.

with the Hubbard mean-field model (TB+U). The Hamiltonian, which encompasses both models, is [111]

$$H = \sum_{i,\sigma} \varepsilon \hat{c}_{i,\sigma}^\dagger \hat{c}_{i,\sigma} + \sum_{\langle i,j \rangle, \sigma} t_1 \left(\hat{c}_{i,\sigma}^\dagger \hat{c}_{j,\sigma} + \hat{c}_{j,\sigma}^\dagger \hat{c}_{i,\sigma} \right) + U \sum_i \hat{n}_{i,\uparrow} \hat{n}_{i,\downarrow} \quad (2)$$

where $\hat{c}_{i,\sigma}^\dagger$ and $\hat{c}_{i,\sigma}$ are creation and annihilation operators of an electron with spin $\sigma = \uparrow, \downarrow$ at site i , respectively, $\hat{n}_{i,\sigma} = \hat{c}_{i,\sigma}^\dagger \hat{c}_{i,\sigma}$ is the number operator for an electron with spin σ at site i , ε is the on-site energy that can be set to zero for all lattice sites and spin directions without loss of generality ($\varepsilon = 0$), $t_1 = 3.12$ eV [112] is the nearest-neighbor hopping integral. We note here that t_1 varies for different structures [113, 114], therefore, in what follows, we will use dimensionless energy units, E/t_1 , where E is the eigenstate energy. U is the on-site Coulomb repulsion. $U/t_1 \sim 1.3$ usually gives good agreement with the generalized gradient approximation to density functional theory [115] (note that slightly different values, such as $U/t_1 \sim 1.6$ as an effective interaction, have also been reported [116]). In the mean-field approximation the 3-rd term of H in Eq. (2) reduces to

$$U \sum_i \left(\hat{n}_{i,\uparrow} \langle \hat{n}_{i,\downarrow} \rangle + \hat{n}_{i,\downarrow} \langle \hat{n}_{i,\uparrow} \rangle - \langle \hat{n}_{i,\uparrow} \rangle \langle \hat{n}_{i,\downarrow} \rangle \right), \quad (3)$$

where $\langle \dots \rangle$ stands for an average, leading to a coupled spin-up and -down eigenproblems to be solved self-consistently via iterations, starting from some initial assumption. The problem is solved using *TB-pack* package [117]. The 32×32 k -grid is used in TB and TB+U calculations. In the TB+U calculations, the occupation numbers convergence threshold and smearing temperature are set as 10^{-5} and $T = 30$ K, respectively.

Figure 3 displays the electronic properties of the GNM in question. The TB bands plotted along a k -path through the high symmetry points presented in Figure 3(a) contain two flat bands at $E_F = 0$ eV. As can be seen in Figure 3(b), the flat bands are truly flat throughout the Brillouin zone. The TB+U

calculations in Figure 3(c, d) for the ferromagnetic (FM) and antiferromagnetic (AFM) initial spin configurations show spin-polarizations, as expected from the Stoner-Hubbard criterion [4, 5, 6]: $U\rho \gg 1$, where ρ is the density of states at the Fermi level. The AFM configuration has a lower energy compared to the FM configuration by $0.053t_1$. Thus, in agreement with Lieb's theorem [28] and Ovchinnikov's rule [118], both stating that the ground state spin configuration of the Hubbard model on a bipartite lattice is $S = |N_A - N_B|/2$, the AFM configuration is the ground state of the system. The atomic site magnetization, shown in Figure 3(e), demonstrates that non-zero magnetization persists till $\frac{U}{t_1} \rightarrow 0$. The largest on-site magnetization at $\frac{U}{t_1} \rightarrow 0$ exceeds 0.2 for zigzag graphene nanoribbons [119].

The general spin lattice built on the localized spin-density "gravity" centers presented in Figure 3(d) can be described by Heisenberg exchange Hamiltonian similar to other lattices such as the one in yttrium iron garnet [120, 121]. The model Hamiltonian reads

$$\begin{aligned} \mathcal{H} = & -\frac{1}{2} \sum_{n=1}^N J_{aa} \mathbf{S}_a(\mathbf{r}_{na}) \sum_{\delta_2} \mathbf{S}_a(\mathbf{r}_{na} + \delta_2) - \\ & -\frac{1}{2} \sum_{n=1}^N J_{bb} \mathbf{S}_b(\mathbf{r}_{nb}) \sum_{\delta_2} \mathbf{S}_b(\mathbf{r}_{nb} + \delta_2) - \\ & - \sum_{n=1}^N \mathbf{S}_a(\mathbf{r}_{na}) [J_{ab} \mathbf{S}_b(\mathbf{r}_{na} + \delta_1) + J'_{ab} \mathbf{S}_b(\mathbf{r}_{na} + \delta_3)], \end{aligned} \quad (4)$$

where a and b denote the two sublattices of the spin lattice (two spins in the unit cell of the structure, S_a and S_b , are generally treated as different for a while):

$$\begin{array}{cccc} & & \vdots & \\ & & \circledast & \\ & & \circledast & \\ \dots & \begin{array}{|c|c|c|c|} \hline \circledast_a & \circledast_a & \circledast_a & \circledast_a \\ \hline \otimes_b & \otimes_b & \otimes_b & \otimes_b \\ \hline \circledast_a & \circledast_a & \circledast_a & \circledast_a \\ \hline \otimes_b & \otimes_b & \otimes_b & \otimes_b \\ \hline \end{array} & \dots \\ & & \vdots & \end{array},$$

where \otimes and \circledast symbols denote spin-down and -up, respectively, J 's stand for the exchange couplings between nearest-neighbor spins of the corresponding sublattices, $'$ is used to distinguish intercellular coupling from the intracellular one, where confusion can arise, δ 's denote direction vectors to the nearest neighbors: 1 - intracellular (pointing down \downarrow), 2 - intercellular horizontal (pointing right \rightarrow), 3 - intercellular vertical (pointing up \uparrow). N is the number of the unit cells in the spin lattice. By switching to ladder operators $S^\pm = S_x \pm iS_y$, one can introduce a linearized Holstein-Primakoff transform [122]:

$$\begin{aligned} S_a^z &= S_a - \mathbf{a}^\dagger \mathbf{a} & S_a^+ &= \sqrt{2S_a - \mathbf{a}^\dagger \mathbf{a}} \mathbf{a} \approx \sqrt{2S_a} \mathbf{a} \\ S_b^z &= \mathbf{b}^\dagger \mathbf{b} - S_b & S_b^+ &= \mathbf{b}^\dagger \sqrt{2S_b - \mathbf{b}^\dagger \mathbf{b}} \approx \mathbf{b}^\dagger \sqrt{2S_b}, \end{aligned} \quad (5)$$

where $S_{a,b}^- = (S_{a,b}^+)^{\dagger}$, and rewrite Hamiltonian in Eq. (4) in terms of $\mathbf{a}(\mathbf{a}^\dagger)$ and $\mathbf{b}(\mathbf{b}^\dagger)$, which are the annihilation (creation) operators for the bosonic magnon excitations on sublattices a and b , respectively. Note that Eqs. (5) accounts for antiferromagnetic ordering on sublattices a and b . Then transforming thus-obtained Hamiltonian into \mathbf{k} -space by Fourier transforms:

$$\mathbf{a}_{nj} = \frac{1}{\sqrt{N}} \sum_{\mathbf{k}} \mathbf{a}_{\mathbf{k}} e^{i\mathbf{k}\mathbf{r}_{nj}}; \quad \mathbf{b}_{nj} = \frac{1}{\sqrt{N}} \sum_{\mathbf{k}} \mathbf{b}_{\mathbf{k}} e^{i\mathbf{k}\mathbf{r}_{nj}}, \quad (6)$$

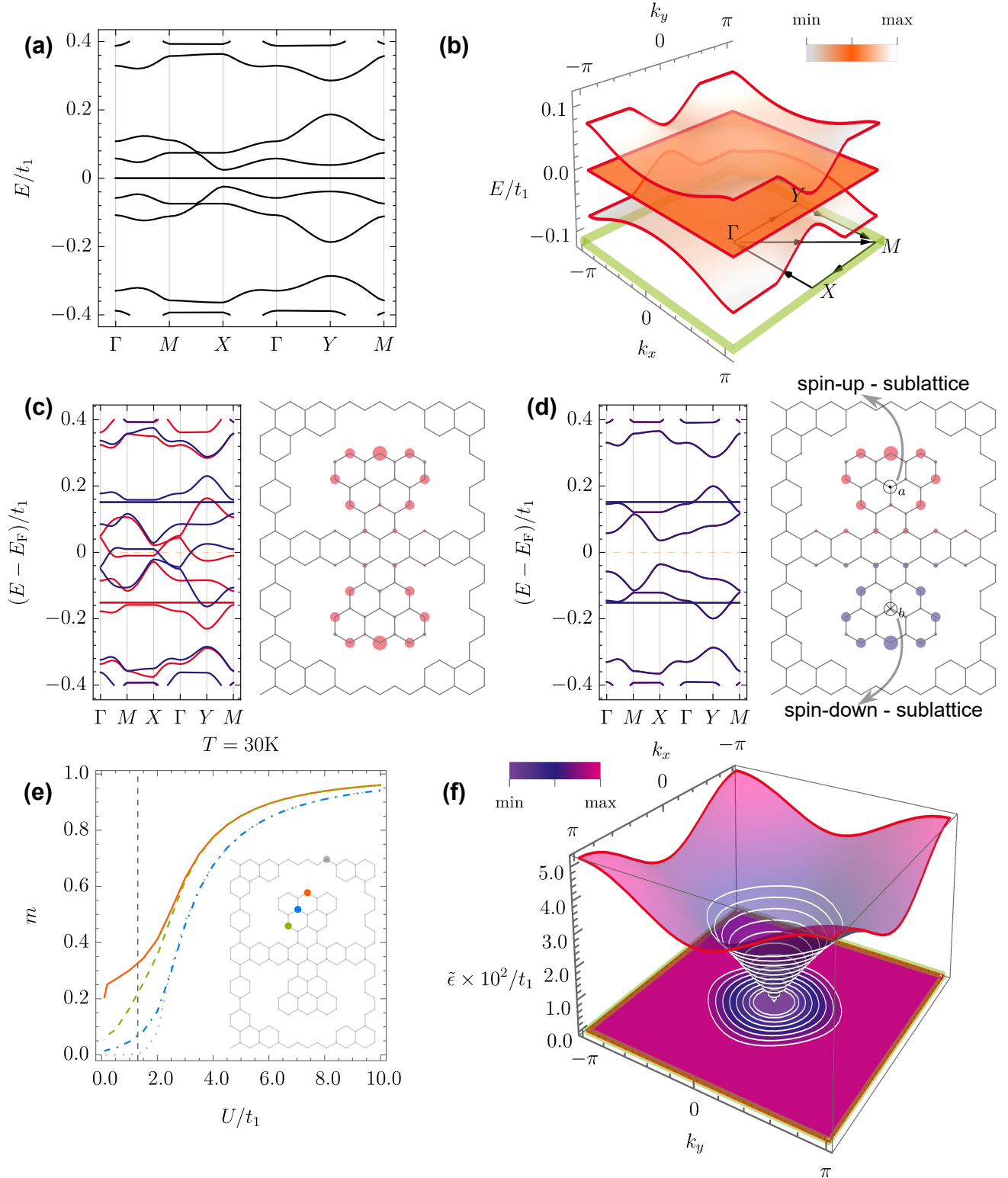


Figure 3: Flat bands and magnetism. (a) The TB energy bands along a 1D k -path through the high symmetry points. (b) The 2D plot of the four TB bands closest to the Fermi level. Light green: Brillouin zone. Black arrows: the k -path through the high symmetry points. (c) The TB+U band structure and the spin density for the initial FM spin configuration. Spin-up and -down species are presented by red and blue, accordingly. Dashed orange line marks the Fermi level adjusted to zero. (d) Same as panel (c) but for the initial AFM spin configuration. \odot_a and \otimes_b mark positions of the spin-up and down gravity centers, respectively. (e) The magnetization of lattice sites highlighted in the inset versus U . Dashed gray vertical line denotes the U -value used in panels (c) and (d). (f) The magnon dispersion from Eq. (18). $\tilde{\epsilon} = 0$ plane of the 3D plot hosts a 2D contour plot of the dispersion with the same color scheme. Light green: Brillouin zone. White: iso-energy curves.

where $j = a, b$ stands for the lattice site, we get a tight-binding-like Bogoliubov-de Gennes Hamiltonian:

$$\mathcal{H}(\mathbf{k}) = \mathcal{H}_0 + \mathcal{H}_1(\mathbf{k}) \quad (7)$$

$$\mathcal{H}_0 = N [(J_{ab} + J'_{ab}) S_a S_b - J_{aa} S_a^2 - J_{bb} S_b^2] \quad (8)$$

$$\mathcal{H}_1(\mathbf{k}) = \sum_{\mathbf{k}} A(\mathbf{k}) \mathbf{a}_{\mathbf{k}}^\dagger \mathbf{a}_{\mathbf{k}} + \sum_{\mathbf{k}} B(\mathbf{k}) \mathbf{b}_{\mathbf{k}}^\dagger \mathbf{b}_{\mathbf{k}} + \left[\sum_{\mathbf{k}} C(\mathbf{k}) \mathbf{a}_{\mathbf{k}} \mathbf{b}_{-\mathbf{k}} + \text{h.c.} \right] \quad (9)$$

where \mathcal{H}_0 is the classical (Ising) ground state energy and $\mathcal{H}_1(\mathbf{k})$ is the magnon dispersion and

$$A(\mathbf{k}) = 2J_{aa} S_a [1 - \cos(\mathbf{k}\boldsymbol{\delta}_2)] - (J_{ab} + J'_{ab}) S_b \quad (10)$$

$$B(\mathbf{k}) = 2J_{bb} S_b [1 - \cos(\mathbf{k}\boldsymbol{\delta}_2)] - (J_{ab} + J'_{ab}) S_a \quad (11)$$

$$C(\mathbf{k}) = -\sqrt{S_a S_b} (J_{ab} e^{-i\mathbf{k}\boldsymbol{\delta}_1} + J'_{ab} e^{-i\mathbf{k}\boldsymbol{\delta}_3}) . \quad (12)$$

Given that $A^*(\mathbf{k}) = A(-\mathbf{k})$, $B^*(\mathbf{k}) = B(-\mathbf{k})$, and $C^*(\mathbf{k}) = C(-\mathbf{k})$. Bosonic diagonalization of \mathcal{H}_1 , which relies on paraunitary transform [123], is equivalent to the standard eigenvalue problem:

$$\begin{pmatrix} A & C \\ -C^\dagger & -B \end{pmatrix} \Psi = \epsilon \Psi , \quad (13)$$

which gives half of the eigenvalues of the full bosonic Hamiltonian:

$$\epsilon_{1,2} = \frac{(A - B) \pm \sqrt{(A + B)^2 - 4|C|^2}}{2} \quad (14)$$

The remaining eigenvalues can be obtained by negating the eigenvalues ϵ .

The general model in Eq. (7) can be specialized now to our case by setting $J_{ab} \equiv J_1$, $J'_{ab} \equiv J_3$, $J_{aa} = J_{bb} \equiv J_2$, $S_a = S_b \equiv S$. Thence, we have

$$\tilde{\epsilon}_{1,2} = \pm \sqrt{\mathcal{A}^2(\mathbf{k}) - |\mathcal{C}(\mathbf{k})|^2} \quad (15)$$

$$\mathcal{A}(\mathbf{k}) = \{2J_2 [1 - \cos(\mathbf{k}\boldsymbol{\delta}_2)] - J_1 - J_3\} S \quad (16)$$

$$\mathcal{C}(\mathbf{k}) = - (J_1 e^{-i\mathbf{k}\boldsymbol{\delta}_1} + J_3 e^{-i\mathbf{k}\boldsymbol{\delta}_3}) S \quad (17)$$

or, equivalently,

$$\tilde{\epsilon}_{1,2} = \pm S \sqrt{\{J_1 + J_3 - 2J_2 [1 - \cos(\mathbf{k}\boldsymbol{\delta}_2)]\}^2 - J_1^2 - J_3^2 - 2J_1 J_3 \cos[\mathbf{k}(\boldsymbol{\delta}_1 - \boldsymbol{\delta}_3)]} . \quad (18)$$

The dispersion relation in Eq. (18), comprises two important limiting cases. If $J_1 = J_3 = 0$ then $\tilde{\epsilon}_{1,2} = \pm 2J_2 S [1 - \cos(\mathbf{k}\boldsymbol{\delta}_2)]$, which is a typical 1D FM magnon dispersion. On the other hand, if $J_2 = 0$, $J_3 = J_1$, and $\boldsymbol{\delta}_3 = -\boldsymbol{\delta}_1$, Eq. (18) yields $\tilde{\epsilon}_{1,2} = \pm 2|J_1|S |\sin(\mathbf{k}\boldsymbol{\delta}_1)|$, wherein the 1D AFM magnon dispersion is readily recognized. Thus, the topologically frustrated GNM in question possesses anisotropic magnon dispersion combining FM and AFM magnons.

The exchange couplings J_1 , J_2 and J_3 can be estimated by relating the classical ground state energies per unit cell \mathcal{H}_0/N , see Eq. (8), to the total energies obtained within the TB+U model, similar to what is done Refs. [124, 125]. For the four configurations:

<table style="border-collapse: collapse; width: 100%;"> <tr><td style="padding: 2px 5px;">⊙₁</td><td style="padding: 2px 5px;">⊙</td><td style="padding: 2px 5px;">⊙</td><td style="padding: 2px 5px;">⊙</td></tr> <tr><td style="padding: 2px 5px;">⊗₂</td><td style="padding: 2px 5px;">⊗₃</td><td style="padding: 2px 5px;">⊗</td><td style="padding: 2px 5px;">⊗</td></tr> <tr><td style="padding: 2px 5px;">⊙₄</td><td style="padding: 2px 5px;">⊙</td><td style="padding: 2px 5px;">⊙</td><td style="padding: 2px 5px;">⊙</td></tr> <tr><td style="padding: 2px 5px;">⊗</td><td style="padding: 2px 5px;">⊗</td><td style="padding: 2px 5px;">⊗</td><td style="padding: 2px 5px;">⊗</td></tr> </table>	⊙ ₁	⊙	⊙	⊙	⊗ ₂	⊗ ₃	⊗	⊗	⊙ ₄	⊙	⊙	⊙	⊗	⊗	⊗	⊗	<table style="border-collapse: collapse; width: 100%;"> <tr><td style="padding: 2px 5px;">⊙₁</td><td style="padding: 2px 5px;">⊙</td><td style="padding: 2px 5px;">⊙</td><td style="padding: 2px 5px;">⊙</td></tr> <tr><td style="padding: 2px 5px;">⊙₂</td><td style="padding: 2px 5px;">⊙₃</td><td style="padding: 2px 5px;">⊙</td><td style="padding: 2px 5px;">⊙</td></tr> <tr><td style="padding: 2px 5px;">⊙₄</td><td style="padding: 2px 5px;">⊙</td><td style="padding: 2px 5px;">⊙</td><td style="padding: 2px 5px;">⊙</td></tr> <tr><td style="padding: 2px 5px;">⊙</td><td style="padding: 2px 5px;">⊙</td><td style="padding: 2px 5px;">⊙</td><td style="padding: 2px 5px;">⊙</td></tr> </table>	⊙ ₁	⊙	⊙	⊙	⊙ ₂	⊙ ₃	⊙	⊙	⊙ ₄	⊙	⊙	⊙	⊙	⊙	⊙	⊙	<table style="border-collapse: collapse; width: 100%;"> <tr><td style="padding: 2px 5px;">⊙₁</td><td style="padding: 2px 5px;">⊙</td><td style="padding: 2px 5px;">⊙</td><td style="padding: 2px 5px;">⊙</td></tr> <tr><td style="padding: 2px 5px;">⊗₂</td><td style="padding: 2px 5px;">⊗₃</td><td style="padding: 2px 5px;">⊗</td><td style="padding: 2px 5px;">⊗</td></tr> <tr><td style="padding: 2px 5px;">⊗₄</td><td style="padding: 2px 5px;">⊗</td><td style="padding: 2px 5px;">⊗</td><td style="padding: 2px 5px;">⊗</td></tr> <tr><td style="padding: 2px 5px;">⊙</td><td style="padding: 2px 5px;">⊙</td><td style="padding: 2px 5px;">⊙</td><td style="padding: 2px 5px;">⊙</td></tr> </table>	⊙ ₁	⊙	⊙	⊙	⊗ ₂	⊗ ₃	⊗	⊗	⊗ ₄	⊗	⊗	⊗	⊙	⊙	⊙	⊙	<table style="border-collapse: collapse; width: 100%;"> <tr><td style="padding: 2px 5px;">⊙₁</td><td style="padding: 2px 5px;">⊗</td><td style="padding: 2px 5px;">⊙</td><td style="padding: 2px 5px;">⊗</td></tr> <tr><td style="padding: 2px 5px;">⊗₂</td><td style="padding: 2px 5px;">⊙₃</td><td style="padding: 2px 5px;">⊗</td><td style="padding: 2px 5px;">⊙</td></tr> <tr><td style="padding: 2px 5px;">⊙₄</td><td style="padding: 2px 5px;">⊗</td><td style="padding: 2px 5px;">⊙</td><td style="padding: 2px 5px;">⊗</td></tr> <tr><td style="padding: 2px 5px;">⊗</td><td style="padding: 2px 5px;">⊙</td><td style="padding: 2px 5px;">⊗</td><td style="padding: 2px 5px;">⊙</td></tr> </table>	⊙ ₁	⊗	⊙	⊗	⊗ ₂	⊙ ₃	⊗	⊙	⊙ ₄	⊗	⊙	⊗	⊗	⊙	⊗	⊙
⊙ ₁	⊙	⊙	⊙																																																																
⊗ ₂	⊗ ₃	⊗	⊗																																																																
⊙ ₄	⊙	⊙	⊙																																																																
⊗	⊗	⊗	⊗																																																																
⊙ ₁	⊙	⊙	⊙																																																																
⊙ ₂	⊙ ₃	⊙	⊙																																																																
⊙ ₄	⊙	⊙	⊙																																																																
⊙	⊙	⊙	⊙																																																																
⊙ ₁	⊙	⊙	⊙																																																																
⊗ ₂	⊗ ₃	⊗	⊗																																																																
⊗ ₄	⊗	⊗	⊗																																																																
⊙	⊙	⊙	⊙																																																																
⊙ ₁	⊗	⊙	⊗																																																																
⊗ ₂	⊙ ₃	⊗	⊙																																																																
⊙ ₄	⊗	⊙	⊗																																																																
⊗	⊙	⊗	⊙																																																																

(19)

where our exchange couplings are obviously $J_1 = J_{12}$, $J_2 = J_{23}$, $J_3 = J_{24}$, one has (in order from left to right)

$$\begin{aligned} J_1 S^2 + J_3 S^2 - 2J_2 S^2 &= E_1 - E_0 , \\ -J_1 S^2 - J_3 S^2 - 2J_2 S^2 &= E_2 - E_0 , \\ J_1 S^2 - J_3 S^2 - 2J_2 S^2 &= E_3 - E_0 , \\ J_1 S^2 + J_3 S^2 + 2J_2 S^2 &= E_4 - E_0 , \end{aligned} \quad (20)$$

Table 1: The summary of the spin lattice energy (in terms of t_1) and structural parameters.

J_1	J_2	J_3	E_0	E_1 (AFM)	E_2 (FM)	E_3	E_4	δ_1/δ_3
-0.0914	0.0061	-0.0142	-176.949	-176.978	-176.925	-176.971	-176.972	0.65

where E_0 is the spin-independent part of a total energy, E_{1-4} are the total energies per two-spins unit cell extracted from TB+U model in the mean-field approximation (four-spins unit cell energies are divided by 2 to obtain E_3 and E_4). Note that E_0 is the fourth unknown along with J_1 , J_2 , and J_3 in the above set of simultaneous Eqs. (20), therefore, it has a unique solution. $S = 1/2$ is the spin of an unpaired electron. Here we neglect fluctuations that are known to lower the classical energy of AFM configurations with respect to FM ones [76]. The nearest-neighbor vectors $\delta_{1,2,3}$ can be found by setting spin positions as gravity centers for positive and negative on-site magnetizations, as shown in Figure 3(d). Figure 3(f) presents the positive branch of the magnon dispersion in Eq. (18) with the parameters given in Table 1. Although some anisotropy is clearly observable, the magnon dispersion is AFM in nature with $\sin(\mathbf{k}\delta) \sim k$ at the Γ point, as indicated by a Dirac cone. This characteristic can be attributed to the gentle J_2 exchange coupling. By setting $t_1 \approx 3$ eV and contrasting the exchange couplings with the room temperature energy (26 meV) and Landauer limit for the minimum energy dissipation per bit ($k_B T \ln(2) \approx 18$ meV, where $k_B = 8.617 \times 10^{-2}$ meV/K is the Boltzmann constant, $T = 300$ K is the room temperature) [126], one sees that the found couplings, even J_2 , are large enough to promise near room-temperature spintronic operations. While our values can be slightly overestimated due to the simplicity of the model used, they are well within the range of experimental values reported for the topologically frustrated Clar's goblet (23 meV) [88]. For comparison, the largest exchange coupling in yttrium iron garnet is about 6 meV [127]. The found coupling energies also belong to the terahertz frequency energy range ($4 \text{ meV} \propto 1 \text{ THz}$), which means that the spin-wave excitations must be responsive and exhibit ultrafast dynamics, thus adding topologically frustrated GNM magnonics to the pool of candidates to bridge the THz gap [128]. Although such meshes can be challenging for synthesis and maintenance due to the high reactivity of zigzag (acene) edges, they could be stabilized upon encapsulation between two hexagonal boron nitride monolayers for ambient environment operation. Alternatively, hexagonal boron nitride patches could be used as fillers for vacancy regions [129, 130] or nanopatterning with hydrogen or fluorine [131, 132] could be used to reinforce the structure and design the required topologically frustrated π -electron networks. Thus, in general, such structures shall be deemed realistic and promising for practical applications.

3 Conclusion

In summary, it has been demonstrated that graph-theoretic topological frustration can persist on a torus. This gives rise not only to zero-energy states in toroidal structures such as nanotori but also to flat energy bands at the Fermi level in 1D nanotubes and 2D nanomeshes. The latter exhibits emergent metal-free quantum magnetism. Thus, topological frustration provides a tool for designing and systematically studying strongly correlated exotic phenomena in monolayer graphene avoiding twistrionics with bi- and tri-layers or multilayer stackings in few-layer systems. Since electronic flat bands are expected to result in an elevated superconductivity transition temperature [9, 10, 12, 13, 16, 95, 15, 96, 133], the superconducting phase diagram shall be a subject of future work for such topologically frustrated systems. A totally different but equally appealing can be a research line on the topological frustration in quantum spin liquids and dimerized magnets, i.e. in systems, where each site (atom) of the initial lattice carries an intrinsic spin.

Supporting Information

Supporting Information is available from the Wiley Online Library or from the author.

Acknowledgements

The author thank C. A. Downing, G. E. Volovik, J. Jiang, V. Lauranenka, D. Corona, A. Kamra and

V. R. Shaginyan for useful comments and discussions. V.A.S. was partly supported by HORIZON EUROPE MSCA-2021-PF-01 (Project No. 101065500, TeraExc).

References

- [1] A. Georges, G. Kotliar, W. Krauth, M. J. Rozenberg, *Rev. Mod. Phys.* **1996**, *68*, 1 13.
- [2] P. A. Lee, N. Nagaosa, X.-G. Wen, *Rev. Mod. Phys.* **2006**, *78*, 1 17.
- [3] M. Amusia, V. Shaginyan, *Strongly correlated Fermi systems: A new state of matter*, Springer Tracts in Modern Physics. Springer International Publishing, Cham, **2020**.
- [4] E. C. Stoner, *Proc. R. Soc. London. Ser. A. Math. Phys. Sci.* **1938**, *165*, 922 372.
- [5] E. C. Stoner, *Proc. R. Soc. London. Ser. A. Math. Phys. Sci.* **1939**, *169*, 938 339.
- [6] J. Hubbard, *Proc. R. Soc. London. Ser. A. Math. Phys. Sci.* **1963**, *276*, 1365 238.
- [7] R. Ortiz, G. Catarina, J. Fernández-Rossier, *2D Mater.* **2023**, *10*, 1 015015.
- [8] H. Yu, T. Heine, *Sci. Adv.* **2024**, *10*, 40 eadq7954.
- [9] V. A. Khodel', V. R. Shaginyan, *JEPT Lett.* **1990**, *51*, 9 488.
- [10] G. E. Volovik, *JETP Lett.* **1994**, *59*, 11 798.
- [11] V. Shaginyan, M. Amusia, A. Msezane, K. Popov, *Phys. Rep.* **2010**, *492*, 2 31.
- [12] N. B. Kopnin, T. T. Heikkilä, G. E. Volovik, *Phys. Rev. B* **2011**, *83*, 22 220503.
- [13] N. B. Kopnin, M. Ijäs, A. Harju, T. T. Heikkilä, *Phys. Rev. B* **2013**, *87*, 14 140503.
- [14] P. Esquinazi, T. T. Heikkilä, Y. V. Lysogorskiy, D. A. Tayurskii, G. E. Volovik, *JETP Lett.* **2014**, *100*, 5 336.
- [15] G. E. Volovik, *JETP Lett.* **2018**, *107*, 8 516.
- [16] S. Peotta, P. Törmä, *Nat. Commun.* **2015**, *6*, 1 8944.
- [17] V. R. Shaginyan, A. Z. Msezane, G. S. Japaridze, *Atoms* **2022**, *10*, 3 67.
- [18] V. R. Shaginyan, A. Z. Msezane, M. Y. Amusia, G. S. Japaridze, *Europhys. Lett.* **2022**, *138*, 1 16004.
- [19] H. Tian, X. Gao, Y. Zhang, S. Che, T. Xu, P. Cheung, K. Watanabe, T. Taniguchi, M. Randeria, F. Zhang, C. N. Lau, M. W. Bockrath, *Nature* **2023**, *614*, 7948 440.
- [20] T. Han, Z. Lu, Z. Hadjri, L. Shi, Z. Wu, W. Xu, Y. Yao, A. A. Cotten, O. Sharifi Sedeh, H. Weldeyesus, J. Yang, J. Seo, S. Ye, M. Zhou, H. Liu, G. Shi, Z. Hua, K. Watanabe, T. Taniguchi, P. Xiong, D. M. Zumbühl, L. Fu, L. Ju, *Nature* **2025**, *643*, 8072 654.
- [21] E. Tang, J.-W. Mei, X.-G. Wen, *Phys. Rev. Lett.* **2011**, *106*, 23 236802.
- [22] T. Neupert, L. Santos, C. Chamon, C. Mudry, *Phys. Rev. Lett.* **2011**, *106*, 23 236804.
- [23] Y.-F. Wang, Z.-C. Gu, C.-D. Gong, D. N. Sheng, *Phys. Rev. Lett.* **2011**, *107*, 14 146803.
- [24] D. Sheng, Z.-C. Gu, K. Sun, L. Sheng, *Nat. Commun.* **2011**, *2*, 1 389.
- [25] N. Regnault, B. A. Bernevig, *Phys. Rev. X* **2011**, *1*, 2 021014.

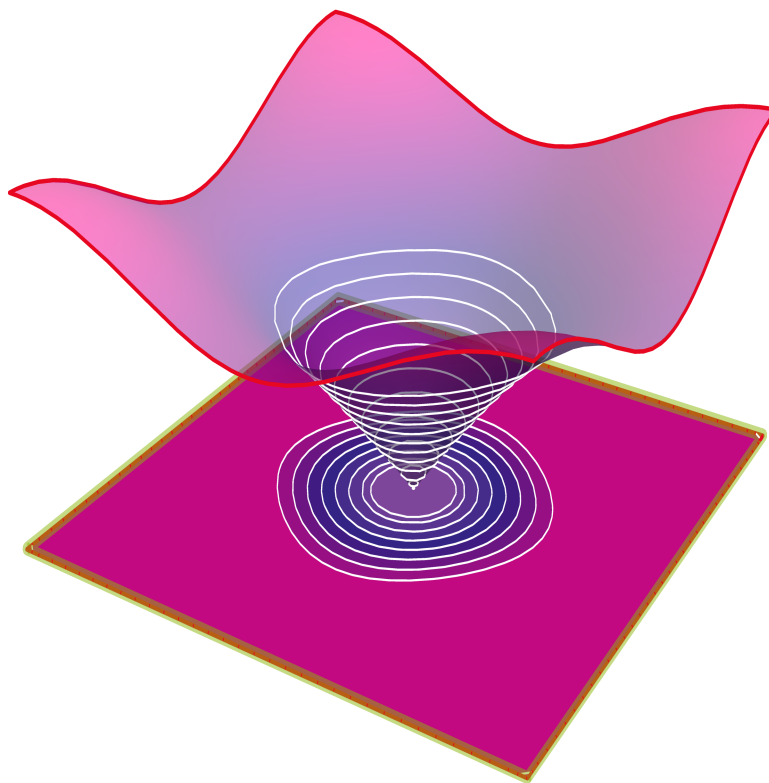
- [26] Y. Shi, B. Xie, F. Ren, X. Cai, Z. Guo, Q. Li, X. Lu, N. Regnault, Z. Liu, J. Liu, *Phys. Rev. Lett.* **2025**, *135*, 25 256603.
- [27] B. Sutherland, *Phys. Rev. B* **1986**, *34*, 8 5208.
- [28] E. H. Lieb, *Phys. Rev. Lett.* **1989**, *62*, 10 1201.
- [29] A. Mielke, *J. Phys. A: Math. Gen.* **1992**, *25*, 16 4335.
- [30] T. Hanisch, B. Kleine, A. Ritzl, E. Müller-Hartmann, *Ann. Phys.* **1995**, *507*, 4 303.
- [31] E. Suárez Morell, J. D. Correa, P. Vargas, M. Pacheco, Z. Barticevic, *Phys. Rev. B* **2010**, *82*, 12 121407.
- [32] D. Green, L. Santos, C. Chamon, *Phys. Rev. B* **2010**, *82*, 7 075104.
- [33] L. Morales-Inostroza, R. A. Vicencio, *Phys. Rev. A* **2016**, *94*, 4 043831.
- [34] T. T. Heikkilä, G. E. Volovik, In *Basic Physics of Functionalized Graphite*, volume 244 of *Springer Series in Materials Science*, 123–143. Springer, Cham, **2016**, URL http://link.springer.com/10.1007/978-3-319-39355-1_6.
- [35] A. Ramachandran, A. Andreanov, S. Flach, *Phys. Rev. B* **2017**, *96*, 16 161104.
- [36] B. Pal, K. Saha, *Phys. Rev. B* **2018**, *97*, 19 195101.
- [37] B. Pal, *Phys. Rev. B* **2018**, *98*, 24 245116.
- [38] A. R. Kolovsky, A. Ramachandran, S. Flach, *Phys. Rev. B* **2018**, *97*, 4 045120.
- [39] J. Mao, S. P. Milovanović, M. Anđelković, X. Lai, Y. Cao, K. Watanabe, T. Taniguchi, L. Covaci, F. M. Peeters, A. K. Geim, Y. Jiang, E. Y. Andrei, *Nature* **2020**, *584*, 7820 215.
- [40] C. V. Morfonios, M. Röntgen, M. Pyzh, P. Schmelcher, *Phys. Rev. B* **2021**, *104*, 3 035105.
- [41] D. Kim, F. Liu, *Phys. Rev. B* **2023**, *385*, 20 205130.
- [42] Y. Zheng, L. Li, X. Wang, Y. Li, N. Luo, W. Ren, L.-M. Tang, Y. Feng, K.-Q. Chen, J. Zeng, *Phys. Rev. B* **2025**, *111*, 4 045118.
- [43] N. Regnault, Y. Xu, M.-R. Li, D.-S. Ma, M. Jovanovic, A. Yazdani, S. S. P. Parkin, C. Felser, L. M. Schoop, N. P. Ong, R. J. Cava, L. Elcoro, Z.-D. Song, B. A. Bernevig, *Nature* **2022**, *603*, 7903 824.
- [44] Y. Cao, V. Fatemi, S. Fang, K. Watanabe, T. Taniguchi, E. Kaxiras, P. Jarillo-Herrero, *Nature* **2018**, *556*, 7699 43.
- [45] Y. Cao, V. Fatemi, A. Demir, S. Fang, S. L. Tomarken, J. Y. Luo, J. D. Sanchez-Yamagishi, K. Watanabe, T. Taniguchi, E. Kaxiras, R. C. Ashoori, P. Jarillo-Herrero, *Nature* **2018**, *556*, 7699 80.
- [46] Y. Cao, D. Rodan-Legrain, O. Rubies-Bigorda, J. M. Park, K. Watanabe, T. Taniguchi, P. Jarillo-Herrero, *Nature* **2020**, *583*, 7699 215.
- [47] J. M. Park, Y. Cao, K. Watanabe, T. Taniguchi, P. Jarillo-Herrero, *Nature* **2021**, *590*, 7845 249.
- [48] F. S. Boi, L. Lei, A. Gu, S. Wang, *Diam. Relat. Mater* **2024**, *148* 111485.
- [49] L. Ye, M. Kang, J. Liu, F. Von Cube, C. R. Wicker, T. Suzuki, C. Jozwiak, A. Bostwick, E. Rotenberg, D. C. Bell, L. Fu, R. Comin, J. G. Checkelsky, *Nature* **2018**, *555*, 7698 638.

- [50] B. R. Ortiz, L. C. Gomes, J. R. Morey, M. Winiarski, M. Bordelon, J. S. Mangum, I. W. H. Oswald, J. A. Rodriguez-Rivera, J. R. Neilson, S. D. Wilson, E. Ertekin, T. M. McQueen, E. S. Toberer, *Phys. Rev. Materials* **2019**, *3*, 9 094407.
- [51] M. Kang, L. Ye, S. Fang, J.-S. You, A. Levitan, M. Han, J. I. Facio, C. Jozwiak, A. Bostwick, E. Rotenberg, M. K. Chan, R. D. McDonald, D. Graf, K. Kaznatcheev, E. Vescovo, D. C. Bell, E. Kaxiras, J. Van Den Brink, M. Richter, M. Prasad Ghimire, J. G. Checkelsky, R. Comin, *Nat. Mater.* **2020**, *19*, 2 163.
- [52] H. Tan, Y. Liu, Z. Wang, B. Yan, *Phys. Rev. Lett.* **2021**, *127*, 4 046401.
- [53] M. Kang, S. Fang, J. Yoo, B. R. Ortiz, Y. M. Oey, J. Choi, S. H. Ryu, J. Kim, C. Jozwiak, A. Bostwick, E. Rotenberg, E. Kaxiras, J. G. Checkelsky, S. D. Wilson, J.-H. Park, R. Comin, *Nat. Mater.* **2022**, *22* 186.
- [54] S.-W. Kim, H. Oh, E.-G. Moon, Y. Kim, *Nat. Commun.* **2023**, *14*, 1 591.
- [55] M. A. Kassem, T. Shiotani, H. Ohta, Y. Tabata, T. Waki, H. Nakamura, *Solid State Commun.* **2024**, *385* 115513.
- [56] R. Pawlak, K. N. Anindya, O. Chahib, J.-C. Liu, P. Hiret, L. Marot, V. Luzet, F. Palmino, F. Chérioux, A. Rochefort, E. Meyer, *ACS Nano* **2025**, *19*, 4 4768.
- [57] Y. Yan, F. Liu, W. Tang, H. X. Wong, B. Qie, S. G. Louie, F. R. Fischer, *Nat. Mater.* **2026**.
- [58] A. Devarakonda, C. S. Koay, D. G. Chica, M. Thinel, A. K. Kundu, Z. Lin, A. B. Georgescu, S. Rossi, S. Y. Han, M. E. Ziebel, M. A. Holbrook, A. Rajapitamahuni, E. Vescovo, K. Watanabe, T. Taniguchi, M. Delor, X. Zhu, A. N. Pasupathy, R. Queiroz, C. R. Dean, X. Roy, *Nat. Phys.* **2025**, *21*, 8 1260.
- [59] D. Bercioux, D. F. Urban, H. Grabert, W. Häusler, *Phys. Rev. A* **2009**, *80*, 6 063603.
- [60] C. E. Whittaker, E. Cancellieri, P. M. Walker, D. R. Gulevich, H. Schomerus, D. Vaitiekus, B. Royall, D. M. Whittaker, E. Clarke, I. V. Iorsh, I. A. Shelykh, M. S. Skolnick, D. N. Krizhanovskii, *Phys. Rev. Lett.* **2018**, *120*, 9 97401.
- [61] C. E. Whittaker, D. R. Gulevich, D. Biegańska, B. Royall, E. Clarke, M. S. Skolnick, I. A. Shelykh, D. N. Krizhanovskii, *Phys. Rev. A* **2021**, *104*, 6 063505.
- [62] Y. Yang, C. Roques-Carmes, S. E. Kooi, H. Tang, J. Beroz, E. Mazur, I. Kaminer, J. D. Joannopoulos, M. Soljačić, *Nature* **2023**, *613*, 7942 42.
- [63] H.-R. Xia, Z. Wang, Y. Wang, Z. Gao, M. Xiao, *Phys. Rev. Lett.* **2025**, *135*, 17 176902.
- [64] S. Nishino, M. Goda, *J. Phys. Soc. Jpn.* **2005**, *74*, 1 393.
- [65] D. L. Bergman, C. Wu, L. Balents, *Phys. Rev. B* **2008**, *78*, 12 125104.
- [66] H.-M. Guo, M. Franz, *Phys. Rev. Lett.* **2009**, *103*, 20 206805.
- [67] H. Tasaki, *Phys. Rev. Lett.* **1995**, *75*, 25 4678.
- [68] H. Tasaki, *J. Stat. Phys.* **1996**, *84*, 3 535.
- [69] K. Kusakabe, M. Maruyama, *Phys. Rev. B* **2003**, *67*, 9 092406.
- [70] M. Kohmoto, Y. Hasegawa, *Phys. Rev. B* **2007**, *76*, 20 205402.
- [71] H. Tasaki, *Eur. Phys. J. B* **2008**, *64*, 3 365.
- [72] P. Miró, M. Audiffred, T. Heine, *Chem. Soc. Rev.* **2014**, *43*, 18 6537.

- [73] W. Ren, P. Boggild, J. M. Redwing, K. S. Novoselov, L. Sun, Y. Qi, K. Jia, Z. Liu, O. Burton, J. A. Alexander-Webber, S. Hofmann, Y. Cao, Y. Long, Q.-H. Yang, D. Li, S. H. Choi, K. K. Kim, Y. H. Lee, M. Li, Q. Huang, Y. Gogotsi, N. Clark, A. Carl, R. Gorbachev, T. Olsen, J. Rosen, K. S. Thygesen, D. K. Efetov, B. S. Jessen, M. Yankowitz, J. Barrier, R. K. Kumar, F. Koppens, H. Deng, X. Li, S. Dai, D. Basov, X. Wang, S. Das, X. Duan, Z. Yu, M. Borsch, A. C. Ferrari, R. Huber, M. Kira, F. Xia, X. Wang, Z.-S. Wu, X. Feng, P. Simon, H.-M. Cheng, B. Liu, Y. Xie, W. Jin, R. R. Nair, Y. Xu, H.-B. Zhang, V. Pellegrini, B. Qu, M. Lemme, A. Katiyar, J.-H. Ahn, I. Aharonovich, M. C. Hersam, S. Roche, Q. Hua, G. Shen, T.-L. Ren, C. M. Koo, N. A. Koratkar, R. J. Young, A. Pollard, *2D Mater.* **2025**.
- [74] X. Meng, C. Qin, X. Liang, G. Zhang, R. Chen, J. Hu, Z. Yang, J. Huo, L. Xiao, S. Jia, *Front. Phys.* **2024**, *19*, 5 53601.
- [75] E. Lieb, D. Mattis, *Phys. Rev.* **1962**, *125*, 1 164.
- [76] P. W. Anderson, *Phys. Rev.* **1952**, *86*, 5 694.
- [77] N. D. Mermin, H. Wagner, *Phys. Rev. Lett.* **1966**, *17*, 22 1133.
- [78] P. C. Hohenberg, *Phys. Rev.* **1967**, *158*, 2 383.
- [79] G. Palle, D. K. Sunko, *J. Phys. A: Math. Theor.* **2021**, *54*, 31 315001.
- [80] K. Y. Cheung, K. Watanabe, Y. Segawa, K. Itami, *Nat. Chem.* **2021**, *13*, 3 255.
- [81] B. Huang, G. Clark, E. Navarro-Moratalla, D. R. Klein, R. Cheng, K. L. Seyler, D. Zhong, E. Schmidgall, M. A. McGuire, D. H. Cobden, W. Yao, D. Xiao, P. Jarillo-Herrero, X. Xu, *Nature* **2017**, *546*, 7657 270.
- [82] C. Gong, L. Li, Z. Li, H. Ji, A. Stern, Y. Xia, T. Cao, W. Bao, C. Wang, Y. Wang, Z. Q. Qiu, R. J. Cava, S. G. Louie, J. Xia, X. Zhang, *Nature* **2017**, *546*, 7657 265.
- [83] C. Wu, D. Bergman, L. Balents, S. Das Sarma, *Phys. Rev. Lett.* **2007**, *99*, 7 070401.
- [84] J. Cayssol, J. N. Fuchs, *J. Phys. Mater.* **2021**, *4*, 3 034007.
- [85] I. Gutman, *Croat. Chem. Acta* **1974**, *46*, 3 209.
- [86] S. J. Cyvin, J. Brunvoll, B. N. Cyvin, *J. Chem. Inf. Model., JCIIM* **1989**, *29*, 4 236.
- [87] S. J. Cyvin, J. Brunvoll, B. N. Cyvin, *J. Math. Chem.* **1990**, *4*, 1 47.
- [88] S. Mishra, D. Beyer, K. Eimre, S. Kezilebieke, R. Berger, O. Gröning, C. A. Pignedoli, K. Müllen, P. Liljeroth, P. Ruffieux, X. Feng, R. Fasel, *Nat. Nanotechnol.* **2020**, *15*, 1 22.
- [89] W. L. Wang, O. V. Yazyev, S. Meng, E. Kaxiras, *Phys. Rev. Lett.* **2009**, *102*, 15 157201.
- [90] H. T. Diep, Frustrated spin systems: History of the emergence of a modern physics, **2025**, URL <http://arxiv.org/abs/2411.12826>, ArXiv; Preprint.
- [91] P. Anderson, *Mater. Res. Bull* **1973**, *8*, 2 153.
- [92] M. Sajjan, R. Gupta, S. S. Kale, V. Singh, K. Kumaran, S. Kais, *J. Phys. Chem. A* **2023**, *127*, 41 8751.
- [93] L. Lovász, M. Plummer, *Matching Theory*, AMS Chelsea Publishing, Providence, Rhode Island, **2009**.
- [94] V. Saroka, On topologically frustrated polymers and where to find them, **2025**, URL <https://doi.org/10.26434/chemrxiv-2025-njj2z>, ChemRxiv; Preprint.

- [95] V. J. Kauppila, F. Aikebaier, T. T. Heikkilä, *Phys. Rev. B* **2016**, *93*, 21 214505.
- [96] T. J. Peltonen, T. T. Heikkilä, *J. Phys.: Condens. Matter* **2020**, *32*, 36 365603.
- [97] J. E. Hopcroft, R. M. Karp, *SIAM J. Comput.* **1973**, *2*, 4 225.
- [98] A. V. Karzanov, In *Trudy Seminara po kombinatornoi matematike*, Voprosy kibernetiki. Izd. Sovetskoe Radio, Moskva, **1973** 66–70, [in Russian].
- [99] L. A. Chernozatonskii, *Phys. Lett. A* **1992**, *170*, 1 37.
- [100] S. Ihara, S. Itoh, *Carbon* **1995**, *33*, 7 931.
- [101] J. R. Sanchez-Valencia, T. Dienel, O. Gröning, I. Shorubalko, A. Mueller, M. Jansen, K. Amsharov, P. Ruffieux, R. Fasel, *Nature* **2014**, *512*, 7512 61.
- [102] S. Bloodworth, R. J. Whitby, *Commun. Chem.* **2022**, *5*, 1 121.
- [103] J. Liu, H. Dai, J. H. Hafner, D. T. Colbert, R. E. Smalley, S. J. Tans, C. Dekker, *Nature* **1997**, *385*, 6619 780.
- [104] C. L. Kane, E. J. Mele, *Phys. Rev. Lett.* **1997**, *78*, 10 1932.
- [105] S. Fajtlowicz, P. E. John, H. Sachs, *Croat. Chem. Acta* **2005**, *78*, 2 195.
- [106] V. A. Saroka, V. A. Demin, M. Pizzochero, Topological engineering of chiral anomalies in Janus nanoribbons, **2026**, URL <https://doi.org/10.26434/chemrxiv-2025-tmvpw>, ChemRxiv; Preprint.
- [107] W. T. Tutte, *J. London Math. Soc.* **1947**, *s1-22*, 2 107.
- [108] C. Berge, *Proc. Natl. Acad. Sci. U.S.A.* **1957**, *43*, 9 842.
- [109] C. Berge, *Comptes Rendus de l'Académie des Sciences, Paris* **1958**, *247* 258.
- [110] J. Edmonds, *Can. J. Math.* **1965**, *17* 449.
- [111] Y. Claveau, B. Arnaud, S. D. Matteo, *Eur. J. Phys* **2014**, *35*, 3 035023.
- [112] B. Partoens, F. M. Peeters, *Phys. Rev. B* **2006**, *74*, 7 075404.
- [113] V. A. Saroka, H. Abdelsalam, V. A. Demin, D. Grassano, S. A. Kuten, A. Pushkarchuk, O. Pulci, *Semiconductors* **2018**, *52*, 14 1890.
- [114] R. B. Payod, D. Grassano, G. N. C. Santos, D. I. Levshov, O. Pulci, V. A. Saroka, *Nat. Commun.* **2020**, *11*, 1 82.
- [115] O. V. Yazyev, *Phys. Rev. Lett.* **2008**, *101*, 3 037203.
- [116] M. Schüler, M. Rösner, T. O. Wehling, A. I. Lichtenstein, M. I. Katsnelson, *Phys. Rev. Lett.* **2013**, *111*, 3 036601.
- [117] V. A. Saroka, TBpack (version 0.6.0 and higher), **2025**, URL <https://github.com/vasilsaroka/TBpack>, Accessed: 2025-12-18.
- [118] A. A. Ovchinnikov, *Theor. Chim. Acta* **1978**, *47*, 4 297.
- [119] M. Fujita, K. Wakabayashi, K. Nakada, K. Kusakabe, *J. Phys. Soc. Jpn.* **1996**, *65*, 7 1920.
- [120] V. Cherepanov, I. Kolokolov, V. L'vov, *Phys. Rep.* **1993**, *229*, 3 81.
- [121] K. Shen, *New J. Phys.* **2018**, *20*, 4 043025.
- [122] T. Holstein, H. Primakoff, *Phys. Rev.* **1940**, *58*, 12 1098.

Table of Contents



Antiferromagnetic magnon dispersion for topologically frustrated graphene nanomesh.

- [123] J. L. van Hemmen, *Z. Phys. B* **1980**, *38*, 3 271.
- [124] J. Jiang, S. G. Louie, *Nano Lett.* **2021**, *21*, 11 197.
- [125] K. N. Anindya, H. Guo, *ACS Nano* **2026**, acsnano.5c22186.
- [126] R. Landauer, *IBM J. Res. & Dev.* **1961**, *5*, 3 183.
- [127] A. J. Princep, R. A. Ewings, S. Ward, S. Tóth, C. Dubs, D. Prabhakaran, A. T. Boothroyd, *npj Quantum Mater.* **2017**, *2*, 1 63.
- [128] R. R. Hartmann, J. Kono, M. E. Portnoi, *Nanotechnology* **2014**, *25*, 32 322001.
- [129] H. S. Wang, L. Chen, K. Elibol, L. He, H. Wang, C. Chen, C. Jiang, C. Li, T. Wu, C. X. Cong, T. J. Pennycook, G. Argentero, D. Zhang, K. Watanabe, T. Taniguchi, W. Wei, Q. Yuan, J. C. Meyer, X. Xie, *Nat. Mater.* **2021**, *20*, 2 202.
- [130] N. V. Tepliakov, R. Ma, J. Lischner, E. Kaxiras, A. A. Mostofi, M. Pizzochero, *Nano Lett.* **2023**, *23*, 14 6698.
- [131] L. A. Chernozatonskii, P. B. Sorokin, *J. Phys. Chem. C* **2010**, *114*, 7 3225.
- [132] F. Withers, T. H. Bointon, M. Dubois, S. Russo, M. F. Craciun, *Nano Lett.* **2011**, *11*, 9 3912.
- [133] L. H. C. M. Nunes, C. M. Smith, *Phys. Rev. B* **2020**, *101*, 22 224514.